

## Effect of trunk length on the flow around a fir tree

Jin-Pyung Lee<sup>1</sup>, Eui-Jae Lee<sup>2</sup> and Sang-Joon Lee<sup>\*2</sup>

<sup>1</sup>*School of Environmental Science and Engineering, Pohang University of Science and Technology, Pohang, 790-784, Korea*

<sup>2</sup>*Department of Mechanical Engineering, Pohang University of Science and Technology, Pohang 790-784, Korea*

*(Received December 7, 2012, Revised September 12, 2013, Accepted September 24, 2013)*

**Abstract.** Flow around a small white fir tree was investigated with varying the length of the bottom trunk (hereafter referred to as bottom gap). The velocity fields around the tree, which was placed in a closed-type wind tunnel test section, were quantitatively measured using particle image velocimetry (PIV) technique. Three different flow regions are observed behind the tree due to the bottom gap effect. Each flow region exhibits a different flow structure as a function of the bottom gap ratio. Depending on the gap ratio, the aerodynamic porosity of the tree changes and the different turbulence structure is induced. As the gap ratio increases, the maximum turbulence intensity is increased as well. However, the location of the local maximum turbulence intensity is nearly invariant. These changes in the flow and turbulence structures around a tree due to the bottom gap variation significantly affect the shelter effect of the tree. The wind-speed reduction is increased and the height of the maximum wind-speed reduction is decreased, as the gap ratio decreases.

**Keywords:** windbreak; white fir tree; shelter effect; wind tunnel; PIV

### 1. Introduction

For centuries, windbreaks have been widely used as natural wind fences to protect crops, orchard trees, and livestock in windy areas. Windbreaks work as a flow resistance to the approaching wind, and force the air to reduce wind speed while accelerating it over the top, providing shelter area near the ground up to some distance downstream of the windbreak (Wang *et al.* 2001). These functional effects are closely related to the flow characteristics of windbreaks.

Raine and Stevenson (1977) measured mean velocities and turbulence intensities of the wake behind various porous fences using a hot-wire anemometer. They classified the wake flow into two regions, bleed-flow dominant and displacement-flow regions. Guan *et al.* (2003) performed a wind tunnel test for a natural windbreak model consisting of trees and shrubs. They estimated the aerodynamic porosity and drag coefficient of the windbreak by measuring the surrounding wind speed. Torita and Satou (2007) measured wind speeds at several points around eight natural shelterbelts with different widths to investigate the fluid mechanical features of wide shelterbelts.

---

\*Corresponding author, Professor, E-mail: [sjlee@postech.ac.kr](mailto:sjlee@postech.ac.kr)

However, the variations in the spatial distributions of mean velocities and turbulence intensities of the wake behind the windbreaks were not be handled.

Gross (1987) investigated the air flow around a single tree numerically. Hagen *et al.* (1981) numerically investigated the effects of width, height, porosity, and other parameters of two-dimensional fences using the  $k-\epsilon$  turbulence model. Bourdin and Wilson (2008) compared the results of 2D and 3D numerical simulations for windbreaks and homogeneous shelterbelts with experimental data. Rosenfeld *et al.* (2010) simulated the flow across several arrangements of trees by employing the steady Reynolds-averaged Navier–Stokes (RANS) equations with assuming windbreaks as homogeneous porous fences.

In previous studies on the windbreak, the porosity was the most important parameter determining the flow characteristics behind the windbreak (Chen *et al.* 2012). However, many parameters affect the shelter effect when the construction of practical windbreaks is considered with trees. Especially, the bottom trunk of a tree creates a gap between the bottom of the tree canopy and the ground surface. This kind of bottom gap is also required in the construction of artificial wind barriers for the transport of vehicles and labor workers at several passages. Therefore, it is important to study the effect of bottom gap on the flow characteristics around a tree, for practical applications. Kim and Lee (2002) investigated the flow fields and shelter effects of porous fences with various bottom gaps using a hybrid particle tracking velocimetry (PTV) velocity field measurement technique. They reported that the region of mean velocity reduction and the shelter effect decrease as the gap ratio increases. However, the results cannot be applied directly to predict the flow behind a real tree because a tree has irregular morphological structures.

In the present study, the flow around a fir tree was investigated experimentally with varying the bottom gap. A fir tree was selected as the model tree, because it has been commonly used as windbreaks in all over the world. The height of the model tree was limited under 20 cm for preventing large blockage effect on the test model. Among several candidate trees, a tree having the most symmetric shape of the canopy was selected as the model. The velocity fields of the wake behind the tree placed in a wind tunnel test section were quantitatively measured using particle image velocimetry (PIV) technique. The variations of shelter effect were estimated and discussed by analyzing the obtained whole velocity field information.

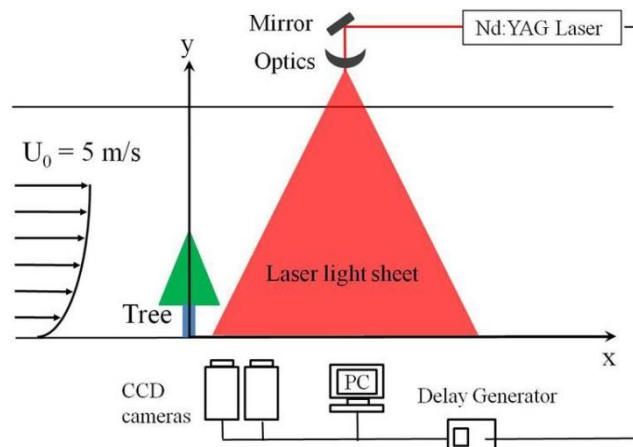


Fig. 1 Schematic diagram of the experimental setup

## 2. Wind-tunnel experiment on windbreak models

### 2.1 Experimental setup

Experiments were performed in a closed-return type of POSTECH subsonic wind tunnel with a test section size of 0.72 m ( $W_{wt}$ )  $\times$  0.65 m ( $H_{wt}$ )  $\times$  8 m ( $L_{wt}$ ). A sharp-edged flat plate of 8 m in length was installed 8 cm above the bottom of the test section. Spires and roughness elements were installed along the spanwise direction to create a neutrally buoyant atmospheric boundary layer. An artificial grass of 0.5 m-fetch-length was placed behind the spire to act as a roughness element for enhancing turbulence intensity. The flow speed ( $U_0$ ) is maintained at 5 m/s. A toothed barrier (Cook 1987) spanning the wind tunnel test section is located near the entry floor of the test section and a biplanar wooden-type grid is installed across the entire test section to yield a logarithmic velocity profile over a significant vertical height of the test section. The turbulence intensity and power spectra were also tried to satisfy the prerequisites for the neutrally stable atmospheric boundary layers.

The experimental set-up and coordinate system are shown in Fig. 1. The PIV system consists of an Nd:YAG pulse laser, four CCD cameras, a delay pulse generator, mirrors and optical lenses for illuminating a thin light sheet and a PC. The Nd:YAG laser has two heads designed for PIV measurements. The maximum energy output of the laser is about 200mJ per pulse. The laser pulse width of 8 nsec makes highly turbulent flows to be frozen in a clear particle image. The laser light sheet of 1 mm thickness is formed by passing the laser beam through cylindrical lenses. Mirrors located at the roof of the wind tunnel test section are used to illuminate the test section. Four high-resolution CCD cameras are positioned perpendicular to the illuminated measurement planes to capture particle images consecutively. A delay generator is used to synchronize the laser and CCD cameras. The time interval between two pulses,  $\Delta t$ , is controlled by using the delay generator. Olive oil droplets of 1~3  $\mu\text{m}$  in mean diameter are used as tracer particles. Compressed air is supplied to the oil chamber to generate tracer particles through a Laskin nozzle and the oil droplets are seeded into the wind tunnel during the experiment.

The mean velocity and turbulence intensity profiles of the simulated ABL were measured using a hot-wire anemometer (TSI IFA-100) at the location of the experimental sample, which is 4.5 m downstream from the leading edge of the test section. For this, X-wire probes were used, and the effective-cosine-law method was employed to calibrate the yaw sensitive (Perry *et al.* 1987, Lim *et al.* 2007). At each measurement point, 16,300 velocity data were acquired at a sampling rate of 2-10 kHz, after low-pass filtering at 800 Hz. The streamwise pressure gradient is nearly negligible due to the presence of corner fillets and small adjustable breathers located at the wind tunnel test section and the first diffuser.

Fig. 2 shows the streamwise mean velocity and turbulence intensity profiles measured at the windbreak location. The mean streamwise velocity normalized by the reference velocity ( $U_{ref}$ ) at a height of  $Y_{ref} = 19$  cm has the power law profile (Eq. (1)). The velocity profile is well fitted with the power law exponent,  $n = 0.16$  and the turbulence intensity is about 20% near the ground surface (Fig. 2). These turbulence intensity and power spectra satisfy the prerequisites for neutrally stable atmospheric boundary layers. The velocity profile of ABL represents the offshore wind coming from sea, and the height is determined using the windbreak near the seashore. The corresponding Reynolds number, based on the model height ( $h$ ), is about  $3.9 \times 10^4$ .

$$\frac{U(y)}{U_{ref}} = \left(\frac{y}{y_{ref}}\right)^n \quad (1)$$

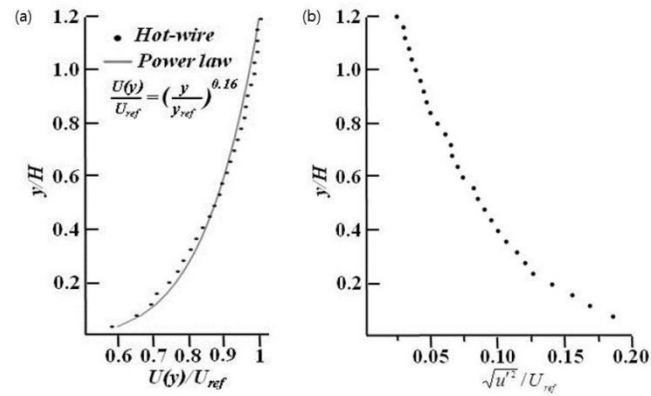


Fig. 2 Profiles of the atmospheric boundary layer of (a) mean velocity and (b) turbulence intensity



Fig. 3 A fir tree model tested in this study

## 2.2 Tree model

Evergreen trees have been used to make windbreak forests for a long time. The stiff needles and soft foliage of evergreens can withstand strong winds. Fir trees are commonly used as windbreaks because of their ability to withstand strong winds in high-temperature regions and to

provide thick shelter zones. In the present study, a five-year-old white fir tree (*Abies concolor*) was used as the model tree. The sample tree was grown according to the standard cultural practices in an open arboretum, where it received full sunlight and water. Fig. 3 shows the configuration and measurement plane for the tree sample. The height ( $H$ ) and width ( $W$ ) of the model tree are 16 cm and 11 cm, respectively.

The bottom gap ( $G$ ) was defined as the vertical distance between the bottom of the tree canopy and the ground surface. The bottom gap ratio represents the ratio of trunk length to canopy height. In Fig. 3, the first branching point was considered as the reference point of the bottom gap. The bottom gap was raised by adjusting the vertical distance of the tree-pod located under the wind tunnel test section. The bottom surface of the test section has a circular hole through which the trunk height can be easily changed. The bottom gap was varied to the bottom gap ratios (ratio of trunk height to canopy height) of  $G/H = 0.0, 0.1, \text{ and } 0.2$ . The optical porosity ( $\beta$ ) of the model tree was estimated to be 0.07. The measurement section is the center vertical plane passing the center of the tree sample.

### 3. Results and discussion

#### 3.1 Flow visualization

Fig. 4 shows contours of the mean velocity and streamlines of the flow around the tree model at three different bottom gap ratios. In front of the tree, the oncoming flow is basically divided into three directions. One direction moves upward and passes over the top of the tree. Another direction goes downward and passes through the bottom gap between the lower canopy of the tree and the ground surface. The other direction just penetrates through the tree canopy. The axial velocity is largely reduced in the leeward of the tree canopy. However, the wind speed is increased in the near-ground region of the bottom gap in spite of ground proximity.

The flow pattern differs depending on the gap ratio. A recirculation flow is formed behind the canopy of the model tree in both cases of  $G/H = 0$  and  $G/H = 0.2$ . At the bottom gap ratio of  $G/H = 0.0$  (Fig. 4(a)), a clockwise large-scale recirculation zone is observed in the leeward side of the canopy in the vertical height ranging from  $y/H = 0.3$  to 0.6 (Fig. 5(a)). Previous experimental and computational studies have reported the formation of recirculation zone located leeward of the dense shelterbelts with porosity of less than 0.3 (Castro 1971, Gross 1987, Heisler and Dewalle 1988, Perera 1981). The recirculation zone had a triangular shape bounded by a line connecting the crest of the shelterbelt and the reattachment point on the ground. However, the recirculation zone formed in the present study has an elliptical shape and the reattachment point does not exist on the ground surface. In the numerical simulations, the canopy of the tree models was assumed to be homogeneously porous. The solid internal structures of a real tree, such as boles, branches, leaves, and others were also supposed to be negligible. Therefore, the recirculation zone of the present study is probably caused mainly by the internal structures of the real tree.

In the case of  $G/H = 0.2$  (Fig. 4(c)), a counter-clockwise large-scale vortex is observed in the leeward side of the canopy in the vertical range of  $y/H = 0.6$  to 1.0 (Fig. 5(b)). The counter-clockwise vortex seems to be caused by the non-uniform local porosity distribution due to the complicated internal branch networks and leaves of the real tree. The structural density in the top part ( $y/H = 0.8$  to 1.0) of the tree is denser than in the middle part ( $y/H = 0.6$  to 0.3), and the local porosity of the middle part is higher than that of the top part. In the middle part of the tree,

the bleed flow which penetrates directly through the canopy inclines upward due to the momentum difference between the two parts of the tree.

However, there is no large-scale recirculation flow in the case of  $G/H = 0.1$  (Fig. 4(b)). For a windbreak with porosity similar to that featured in the present study, air flow in the lower part of the canopy was inclined upward to the upper part, whereas a large-scale recirculation zone was also not observed (Gross 1987, Melese Endalew *et al.* 2009, Rosenfeld *et al.* 2010).

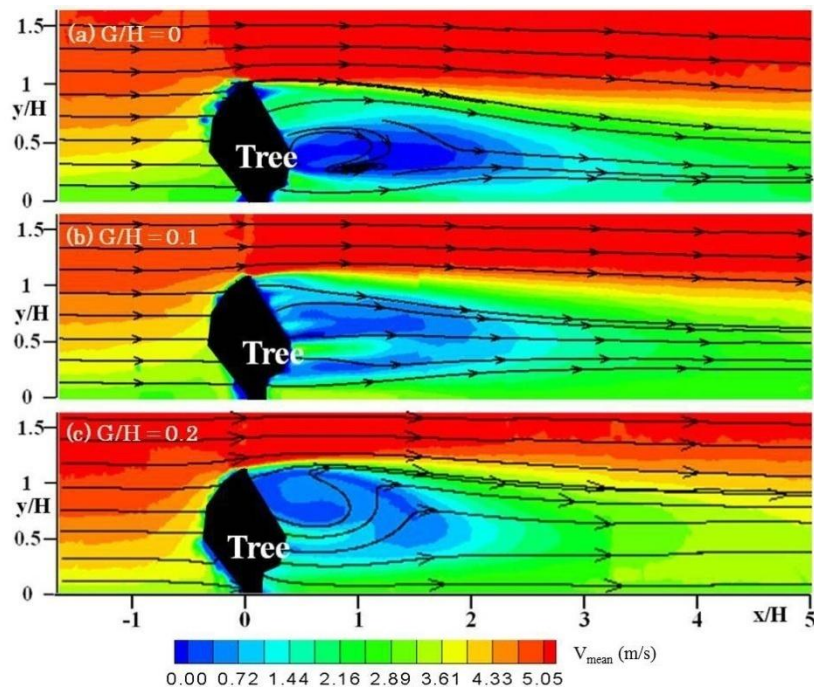


Fig. 4 Mean velocity contours and streamlines in the vertical center plane around a single tree

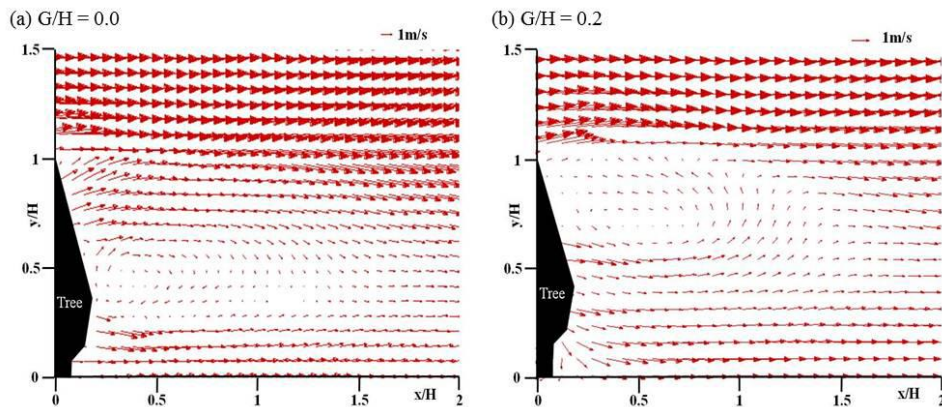


Fig. 5 Velocity vectors ( $u,v$ ) in the vertical center plane of near wake behind the tree

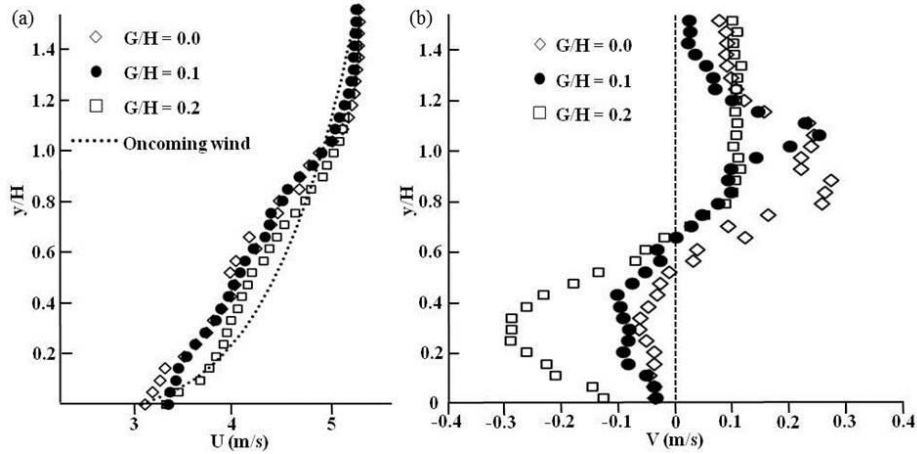


Fig. 6 Mean velocity profiles of (a) streamwise and (b) vertical components measured at  $x/H = -0.5$

### 3.2 Flow and turbulence structure

Fig. 6 represents the mean streamwise and vertical velocity profiles taken from the velocity field data of Fig. 4 at the downstream location of  $x/H = -0.5$ . The presence of the tree slightly changes the mean streamwise velocity profiles, compared to the velocity profiles of the oncoming wind (Fig. 2(a)), which were measured without the tree model at the same location. In the upper region, above  $y/H > 1$ , the streamwise velocity is faster than that of the oncoming wind. However, in the lower region, below  $y/H < 1$ , the streamwise velocity is slower than that of the oncoming wind. When the gap ratio is  $G/H = 0.2$ , the velocity reduction is smallest. However, the gap ratio of  $G/H = 0.0$  exhibits the largest velocity reduction.

The vertical velocity component has negative values in the lower part of the tree, which is below the mid-height ( $0.5 < y/H < 0.7$ ). This indicates that the oncoming wind is divided into two opposite directions at this height of the tree. The separation point varies slightly depending on the length of the bottom gap. When the gap ratio increases, the negative vertical velocity increases, whereas the positive value decreases. In both cases of  $G/H = 0.0$  and  $0.1$ , the magnitudes of the negative vertical velocities are smaller than those of the positive values. The ground surface and bottom gap may induce a sort of flow resistance and prevent the wind heading to the ground. When the gap ratio is  $G/H = 0.0$ , the vertical velocity has a maximum value in the top part of the canopy between  $y/H = 0.7 \sim 1.0$ . The oncoming wind mostly moves over or passes through the top part (Fig. 5(a)). This flow pattern may cause the clockwise recirculation zone shown in Fig. 4(a). At the large gap ratio of  $G/H = 0.2$ , the vertical velocity has large negative values. In addition, the upward flow passing over the crest of the tree is smaller than the downward flow passing through the bottom gap. In this scenario, the bottom gap is wide enough for the flow to pass easily without significant flow resistance. The vertical velocity has maximum negative values in the region of  $y/H = 0.2 \sim 0.4$ . In the gap ratio of  $G/H = 0.2$ , most of the flow moves downward or passes through the lower part of the canopy (Fig. 5(b)). This kind of flow pattern seems to induce the counterclockwise recirculation flow shown in Fig. 4(c).

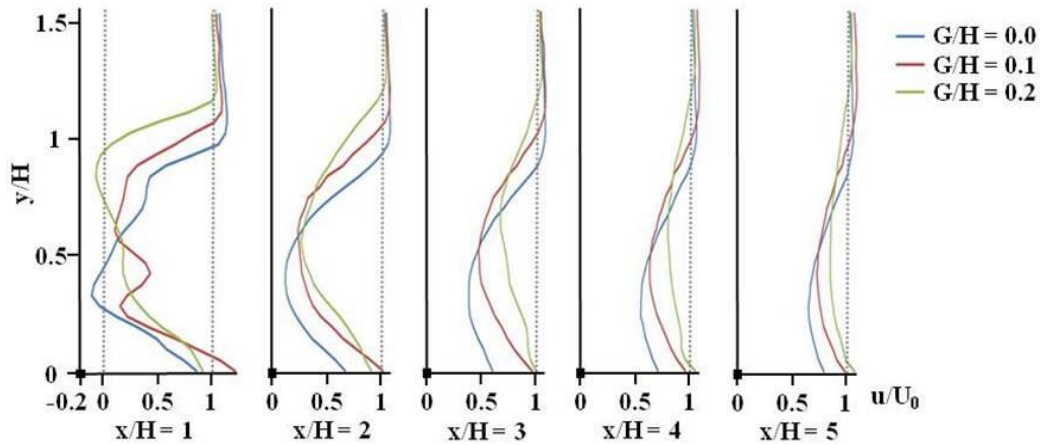


Fig. 7 Variations of mean streamwise velocity profiles along the x-direction

Fig. 7 shows the mean streamwise velocity profiles selected from the mean velocity field at five downstream locations. At  $x/H = 1$ , which is just behind the tree, the streamwise velocity has negative values for the cases of  $G/H = 0.0$  and  $0.1$ . This location belongs to the recirculation zone, as shown in Figs. 4 and 5. In addition, three different flow regions are observed behind the tree. These flow regions comprise two shear layers and one bleed flow region. The upper shear layer is developed from the top of the canopy, whereas the lower shear layer occupies the bottom gap in the near-wake region. The bleed flow passing through the canopy of the model tree makes up the other region. In the upper shear layer ( $y/H > 0.7$ ), the mean streamwise velocity increases as the gap ratio decreases. However, in the lower shear layer ( $y/H < 0.3$ ), the streamwise mean velocity has the maximum value at  $x/H = 2$ , when the gap ratio is  $G/H = 0.1$ . Beyond the downstream location of  $x/H = 2$ , the streamwise velocity increases as the gap ratio increases. Due to the expansion of the shear layers separated from the top and bottom edges of the tree canopy, the streamwise velocity profiles gradually approach the velocity profile ( $U_0$ ) of the oncoming wind as the flow goes downstream, regardless of the gap ratio. Going downstream, the flow recovers its momentum deficit. This recovery rate increases as the gap ratio increases. Eventually, the flow might be restored to its original state at far downstream. When the flow fully recovers the initial momentum, this flow is called the “re-equilibration zone,” in which the velocity perturbations by the windbreaks are smoothed and the undisturbed upstream wind is nearly reestablished (Judd *et al.* 1996).

Depending on the gap ratio, the recovery rates are observed to be different. The difference is probably caused by the different turbulence intensity distributions of the wake. The spatial distributions of turbulence intensities of the streamwise and vertical velocity components are given in Fig. 8. In all the experimental conditions, the turbulence intensities have maximum values in the shear layers developed from the top and bottom gaps of the tree. The location of the local maximum turbulence intensity is nearly invariant, regardless of the gap ratio. In the upper shear layer and in the bleed flow regions, the maximum turbulence intensity values increase as the gap ratio increases. However, in the lower shear layer, when the gap ratio is  $G/H = 0.1$ , the turbulence intensity has maximum values. The small gap of  $G/H = 0.1$  seems to increase the flow speed (Fig. 7) and augment turbulent velocity fluctuations in the lower shear layer. This high-turbulence intensity enhances the recovery of momentum deficit to the freestream wind speed. The region of

large turbulence intensity expands as the flow goes downstream due to the expansion of the shear layer. In the near-wake region ( $x/H < 2$ ), the streamwise turbulence intensity profiles have two peaks, one each in the upper and lower shear layers. The peak in the lower shear layer may be attributed to the interaction between the wall boundary layer and the shear layer separated from the bottom edge of the tree canopy.

The maximum turbulence intensity in the upper shear layer is much larger than that in the lower shear layer. The higher turbulence intensity implies that the recovery rate in the upper shear layer is greater than that in the lower shear layer.

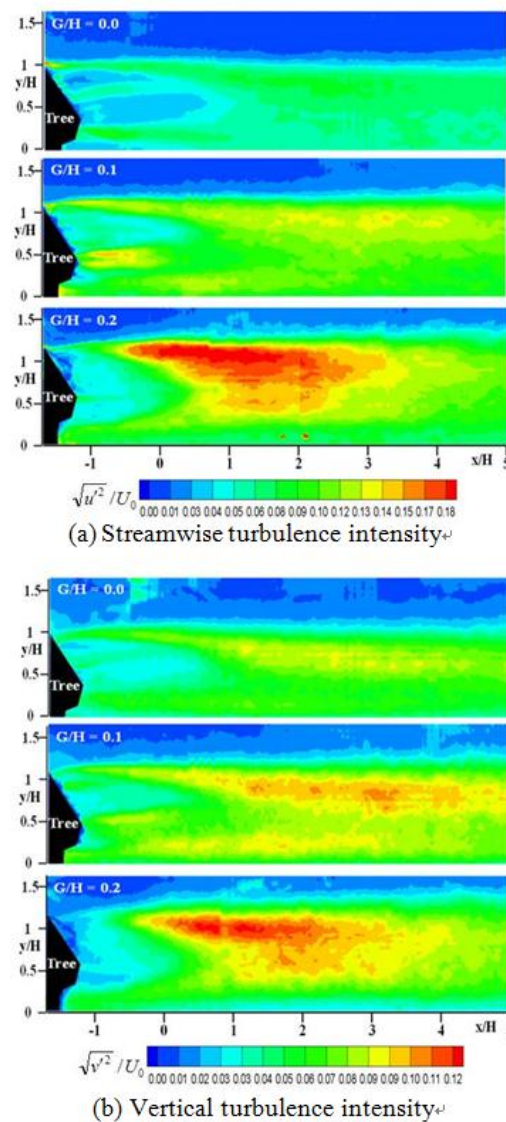


Fig. 8 Spatial distributions of (a) streamwise and (b) vertical turbulence intensities

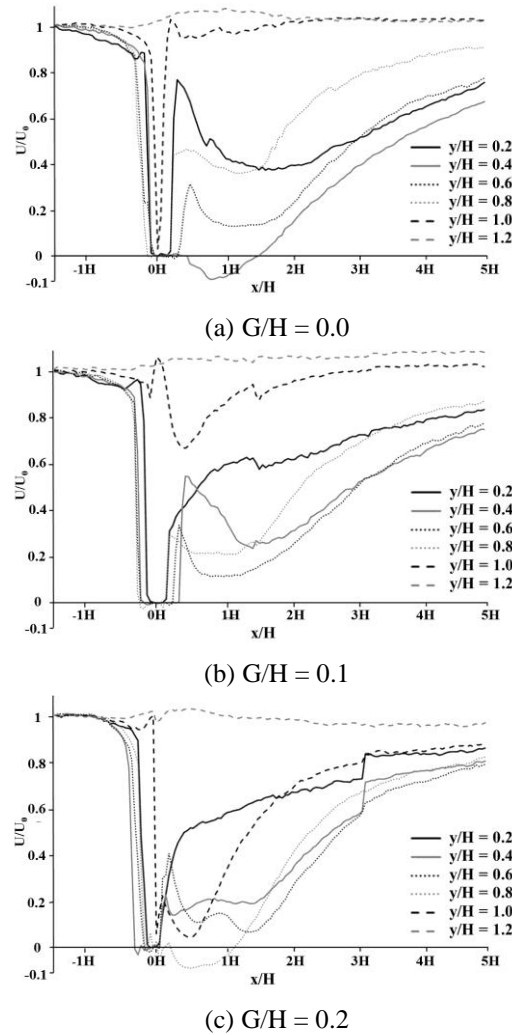


Fig. 9 Variations of axial velocity distributions at several vertical heights normalized by the freestream wind speed  $U_0$

### 3.3 Wind-speed reduction and shelter effect

Variations in axial velocity distributions at several vertical heights normalized by the free stream wind speed  $U_0$  are shown in Fig. 9. The negative values for the cases of  $G/H = 0.0$  and  $0.2$  represent the presence of a recirculation zone. In the horizontal plane of  $y/H = 1.2$  behind the tree canopy, streamwise velocity profiles are similar and the wind-speed reduction does not appear, regardless of the bottom gap ratio. In the height of  $y/H = 1.0$ , the wind speed is increased, as the gap ratio decreases. This phenomenon is caused by the updraft in front of the tree (Fig. 6(b)). The tree canopy makes the updraft as shown in the Fig. 6(b). This updraft accelerates the wind in the top area and the acceleration is increased, as the gap ratio decreased.

The height for best wind-speed reduction is changed according to the gap ratio. For the case of

$G/H = 0.0$ , the height of  $y/H = 0.4$  has the lowest velocity. For the case of  $G/H = 0.1$ , the wind-speed reduction is best in the region between  $y/H = 0.4$  and  $y/H = 0.6$ . For the case of  $G/H = 0.2$ , the heights between  $y/H = 0.4$  and  $y/H = 0.8$  are the best wind-speed reduction region. These regions of wind-speed reduction are called the “quiet zone” (Raine and Stevenson, 1977). The wind speed is low in the quiet zone, providing a very good shelter effect. Behind a 2D wind fence, the quiet zone has a triangular shape bounded by the fence, ground surface, and the line connecting the fence crest to the downstream ground surface,  $x/H \approx 3\sim 7$  (Raine and Stevenson 1977, Judd *et al.* 1996). The tree model tested in this present study has a single stem, forming a massive bottom gap between the canopy of the tree and ground surface. Due to the presence of the bottom gap, the downdraft is created in the front of the tree (Fig. 6(b)) and the wind speed is accelerated in the near-ground region (Fig. 7), resulting in the lifting of the quiet zone in the downstream wake region. Therefore, the height of the best wind-speed reduction is increased as the gap ratio increases.

In the middle height ( $y/H = 0.2\sim 0.8$ ), wind speed is recovered rapidly after passing the windbreak. However, the recovery rate is increased as, the gap ratio increases. In the leeward region behind the tree model of  $G/H = 0.2$ , freestream is easily entrained from the near-ground region ( $y/H = 0\sim 0.2$ ) because of relatively large bottom gap. For the case of  $G/H = 0.0$ , the entrainment of ambient high-speed wind takes time because the ground surface block the entrainment of freestream wind into the wake region. Therefore, the wind-speed reduction of the  $G/H = 0.0$  is great in the middle height.

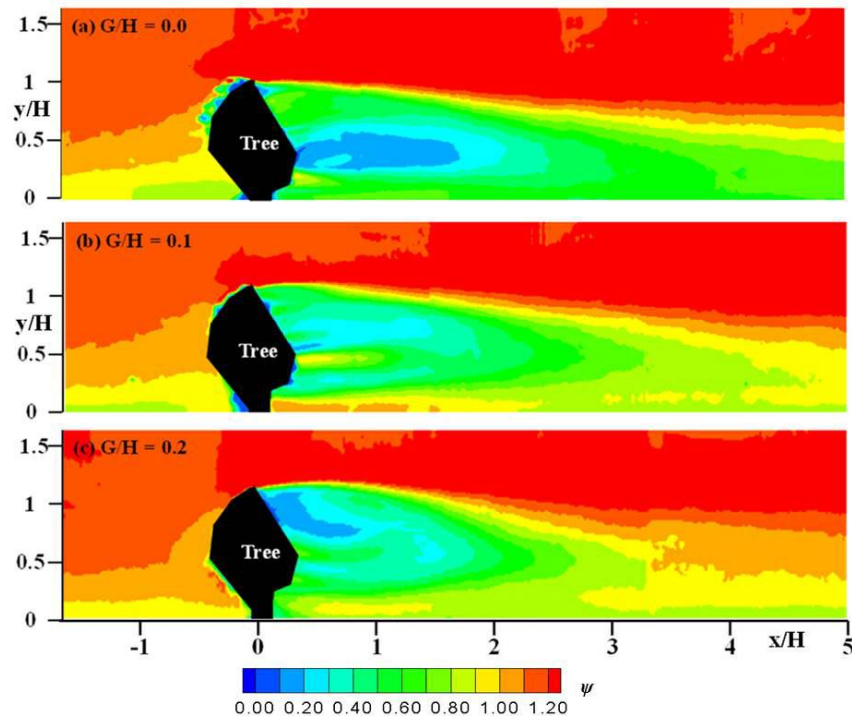


Fig. 10 Contour plots of the shelter parameter for three different bottom gap ratios

The shelter parameter was evaluated to compare the shelter effect quantitatively as a function of the gap ratio. Fig. 10 shows the spatial distribution. The effect of windbreak on sheltering has been expressed by several means in previous studies. The parameter most commonly used is shelter distance ( $d_{20}$ ), in which the wind speed in the leeward is reduced by 20% (van Eimern *et al.* 1964). The minimum wind speed ( $U_{\min}$ ) and its downstream location ( $X_{\min}$ ) was also employed to characterize the shelter effect (Heisler and DeWalle 1988). Although the shelter effect is closely related to spatial distribution of the wind speed, these indices represent only the physical properties of several local points. Therefore, it is not easy to search the region of the best shelter effect using these parameters. In addition, these indices disregard the effect of turbulence intensity, although the turbulence level is an important physical parameter in the estimation of shelter effect of a windbreak on wind erosion and damages.

Gandemer (Perera 1981) proposed a shelter parameter to quantify the shelter effect of a porous fence. However, this parameter reflects only the streamwise mean velocity and turbulence intensity. Although the vertical velocity component is relatively small compared to the streamwise velocity component, it also has to be considered for evaluating the shelter effect accurately. Kim and Lee (2002) proposed a shelter parameter to quantify the shelter effect of a porous fence. This parameter not only reflects streamwise mean velocity but also includes vertical velocity component. Although the vertical velocity component is relatively small compared with the streamwise velocity component, we need to consider the former to accurately evaluate the shelter effect. In this study, the following shelter parameter (Eq. (2)) was employed to take into account the simulated atmospheric boundary layer at each position behind the windbreak

$$\psi(x, y) = \frac{(|U(x, y)| + \sqrt{u(x, y)^2} + |V(x, y)| + \sqrt{v(x, y)^2})}{(U_{ref}(y) + \sqrt{u_{ref}(y)^2})} \quad (2)$$

Fig. 10 shows contour plots of the shelter parameter according to the bottom gap ratio. The contours of the shelter parameter in the upper shear layer look somewhat similar regardless of the bottom gap ratio. The shelter parameter rapidly increases as the flow goes downstream. In the lower shear layer, the middle bottom gap ratio of  $G/H = 0.1$  has large values of shelter parameter ( $\psi (G/H=0.1) > 0.3$ ), because the gap flow passes the bottom gap at a high speed, as shown in Fig. 7. Considering the whole region, the bottom gap ratio of  $G/H = 0$  has the minimum value of shelter parameter. Moreover, the sheltered zone is widest among the three conditions tested in the present study.

The sheltering phenomenon is closely related to the aerodynamic porosity ( $\alpha$ ) of a windbreak. The aerodynamic porosity is the ratio of the mean streamwise wind velocities at immediately windward and leeward of the windbreak (Guan *et al.* 2003, Bitog *et al.* 2009). Since the bleed flow decreases as the bottom gap ratio increases (Fig. 4), the aerodynamic porosity is also decreased in the present study. The smaller porosity may induce higher turbulence, which may enhance the recovery of the mean velocity deficit to the freestream wind speed, thus resulting in a shorter sheltered zone. However, the low turbulence in the lower shear layer may push the re-equilibration zone to the far-wake region and extend the shelter zone toward downstream.

#### 4. Conclusions

The flow structure behind a fir tree was investigated with varying bottom gap ratios using a

PIV velocity field measurement technique. The flow behind a tree was divided into three flow regions: an upper shear layer separated from the canopy crest, a bleed flow passing through the canopy, and a lower shear layer developed from the bottom gap. Each flow region has different flow characteristics as a function of the bottom gap ratio. The bottom gap ratio of  $G/H = 0$  is observed to have a clockwise large-scale recirculation flow in the near-wake region. However, the bottom gap ratio of  $G/H = 0.2$  makes a counterclockwise large-scale recirculation flow.

The leeward flow disturbed by the tree model exhibits different flow patterns as a function of bottom gap ratio. The wake flow gradually recovers momentum deficit to the freestream wind speed as the flow goes downstream. The recovery rate increases as the bottom gap ratio increases due to the high turbulence intensity. The turbulence intensity also increases as the bottom gap ratio increases. However, the location of the local maximum turbulence intensity is nearly invariant, regardless of the bottom gap ratio.

The shelter parameter representing the adverse shelter effect has a different spatial distribution according to the bottom gap ratio. The sheltering phenomenon is closely related to the modified flow characteristics, such as the reduction of wind speed and turbulence intensity caused by the aerodynamic porosity of the tree. The bottom gap ratio of  $G/H = 0$  shows great shelter effect. The ratio of  $G/H = 0.1$  has the worst shelter effect in the lower shear layer. However, critical gap ratio will be changed slightly for another tree, depending on its morphological structure.

## Acknowledgments

This work was supported by the National Research Foundation of Korea(NRF) grant funded by the Korea government (MSIP) (No. 2008-0061991).

## References

- Bitog, J.P., Lee, I.B., Shin, M.H., Hong, S.W., Hwang, H.S., Seo, I.H., Yoo, J.I., Kwon, K.S., Kim, Y.H and Han, J.W. (2009), "Numerical simulation of an array of fences in Saemangeum reclaimed land", *Atmos. Environ.*, **43**(30), 4612-4621.
- Bourdin, P. and Wilson, J.D. (2008), "Windbreak aerodynamics: is computational fluid dynamics reliable?", *Bound.- Lay. Meteorol.*, **126**(2), 181-208.
- Castro, I.P. (1971), "Wake characteristics of two-dimensional perforated plates normal to an airstream", *J. Fluid Mech.*, **46**, 599-609.
- Cleugh, H.A. (1998), "Effects of windbreaks on airflow, microclimates and crop yields", *Agroforest. Syst.*, **41**(1), 55-84.
- Gross, G. (1987), "A numerical study of the air flow within and around a single tree", *Bound.- Lay. Meteorol.*, **40**(4), 311-327.
- Guan, D., Zhang, Y. and Zhu, T. (2003), "A wind-tunnel study of windbreak drag", *Agr. Forest. Meteorol.*, **118**(1-2), 75-84.
- Chen, G., Wang, D., Sun, C. and Li, J. (2012), "3D numerical simulation of wind flow behind a new porous fence", *Powder Technol.*, **230**, 118-126.
- Hagen, J.L., Skidmore, E.L., Miller, P.L. and Kipp, J.E. (1981), "Simulation of effect of wind barriers on airflow", *Trans - ASAE* **24**, 1002-1008.
- Heisler, G.M. and Dewalle, D.R. (1988), "Effects of windbreak structure on wind flow", *Agr. Ecosyst. Environ.*, **22**, 41-69.
- Judd, M.J., Raupach, M.R. and Finnigan, J.J. (1996), "A wind tunnel study of turbulent flow around single

- and multiple windbreaks, part I: Velocity fields”, *Bound. - Lay. Meteorol.*, **80**(1-2), 127-165
- Kim, H.B. and Lee, S.J. (2002), “The structure of turbulent shear flow around a two-dimensional porous fence having a bottom gap”, *J. Fluid. Struct.*, **16**(3), 317-329.
- Melese, E.A., Hertog, M., Delele, M.A., Baetens, K., Persoons, T., Baelmans, M., Ramon, H., Nicolai, B.M. and Verboven, P. (2009) “CFD modelling and wind tunnel validation of airflow through plant canopies using 3D canopy architecture”, *Int. J. Heat Fluid Fl.*, **30**(2), 356-368.
- Perera, M.D.A.S. (1981), “Shelter behind two-dimensional solid and porous fences”, *J. Wind Eng. Ind. Aerod.*, **8**(1-2), 93-104.
- Raine, J.K. and Stevenson, D.C. (1977), “Wind protection by model fences in a simulated atmospheric boundary layer”, *J. Wind Eng. Ind. Aerod.*, **2**(2), 17-39.
- Rosendfeld, M., Marom, G. and Bitan, A. (2010), “Numerical simulation of the airflow across trees in a windbreak”, *Bound. - Lay. Meteorol.*, **135**(1), 89-107.
- Torita, H. and Satou, H. (2007), “Relationship between shelterbelt structure and mean wind reduction”, *Agr. Forest. Meteorol.*, **145**(3-4), 186-194.
- van Eimern, J., Karschon, R., Razumova, L.A. and Robertson, G.W. (1964), *Windbreaks and Shelterbelts*, W.M.O. Tech. Note No. 59.
- Wang, H., Takle, E.S. and Shen, J. (2001) “Shelterbelts and windbreaks: mathematical modeling and computer simulations of turbulent flows”, *Annu. Rev. Fluid Mech.*, **33**, 549-586.